Charge-transfer reactions in atom scattering from ionic surfaces: A time-dependent wavepacket approach

G. R. Darling,[a] Y. Zeiri[b] and R. Kosloff[c]

[a] *Surface Science Research Centre, Department of Chemistry, The University of Liverpool, Liverpool, UK L69 3BX*
[b] *Department of Chemistry, Nuclear Research Center-Negev, P.O. Box 9001, Beer-Sheva 84190, Israel*
[c] *Department of Physical Chemistry and the Fritz Haber Research Center, The Hebrew University, Jerusalem 91904, Israel*

Received 18th May 2000
First published as an Advance Article on the web 11th September 2000

A diabatic description of charge transfer between atoms and ionic surfaces is presented, specifically examining the F/LiF(100) and F/KI(100) systems for which experiment shows ion formation to be very efficient. Potential energy surfaces describing the energetics for these systems have been generated with a semi-empirical scheme. At the site of charge exchange, there is a curve-crossing between the ground state and the state representing charge capture by the projectile. Quantum dynamics calculations with time-dependent wavepacket methods give an initial ion-formation probability of unity for all cases considered. At lowest energies, the ions cannot escape the surface, giving an effective threshold for negative-ion production very close to that observed in experiment. Re-neutralization by charge transfer back to the conduction band of the solid is also examined.

I. Introduction

Charge transfer between an atom and a surface is one of the fundamental processes occurring in gas–surface dynamics. It is best understood on metal surfaces.[1,2] Electron transfer into very low-lying atomic states can be accompanied by ejection of another electron (an Auger mechanism) or emission of light (chemiluminescence), while transfer into atomic affinity levels often occurs by a resonant process. In this paper, we shall focus on resonant transfer between a surface and neutral projectiles. On metal surfaces this is facile because the affinity level of the incoming atom is downshifted by interaction with the electrostatic image charge in the metal surface, as indicated in Fig. 1(a). For low workfunction surfaces, a large fraction of the atoms scatter as negative ions.[2] On surfaces with higher workfunctions (*e.g.* transition metals), if the atoms are directed at grazing incidence (a few degrees from the surface plane) in the hyperthermal energy range ($\sim$keV), the resonance conditions are assisted by a Doppler upshift of the electrons at the Fermi level.[2]

On insulating ionic surfaces, the situation appears less favourable for electron transfer. The valence electrons are tightly bound to the anion sites, leading to narrow bandwidths, low electron mobilities and high workfunctions. The atom affinity level would have to decrease substantially to become resonant with the valence band of the surface, but the image attraction is small (at least for singly-charged ions). One would expect a very low probability of electron transfer, however the

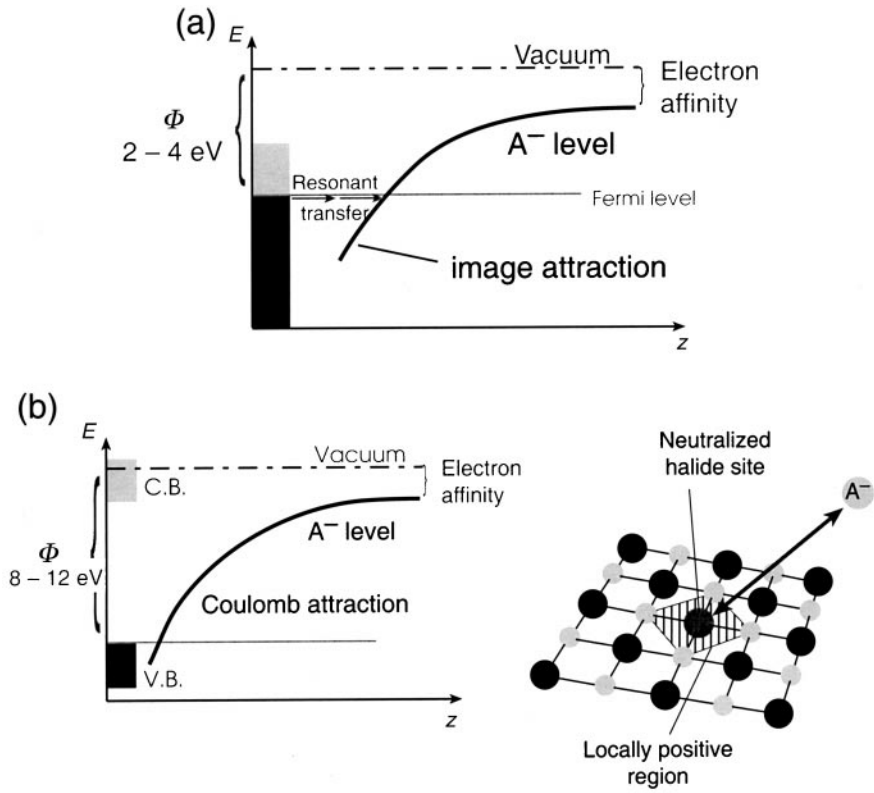

Fig. 1 (a) Schematic of the variation of the atomic affinity level with distance above a metal surface, z. The decrease in energy of the A^- level is due to the interaction with the image charge. Resonant filling can occur when it crosses the Fermi energy. (b) Schematic of the variation of an atomic affinity with distance above an insulating, ionic surface. The work function is very much larger than for a metal, and so the affinity level has further to drop before it can fill resonantly on crossing the top of the valence band. This large drop is effected by a Coulomb attraction between the negative atomic ion and the positively charged region formed on the surface at the site of charge transfer.

opposite has been observed in recent experiments. In grazing incidence scattering experiments with energies up to 100 keV, Winter and coworkers detected very high yields of negative ions for O, and F atoms and positive ions incident on alkali-metal halide surfaces.[3–6] In the scattering of F from KI, for instance, almost complete conversion of neutral atoms into negative ions is observed.[4] Similar results have been seen in scattering of O and F atoms from the MgO(100) surface.[7,8]

A possible explanation of these observations is that the electron is transferred from surface or defect states located in the band-gap of the solid. This would require a much smaller downshift of the affinity level, however, the high yield of negative ions suggests a high density-of-states for these surface/defect states. Complementary studies of the neutralization probability of Na^+ ions show that this is not the case. Such states in the band-gap would be expected to give efficient neutralization, yet experiment finds the Na^+ scatter as positive ions only.[9]

Simple electrostatic considerations show that the high workfunction of an ionic solid is not, in fact, a barrier to charge transfer from the valence band to a scattering atom. The valence electrons are tightly bound to the anionic sites, therefore the charge transfer from surface to atom is largely a local event involving an electron moving on to the atom from a particular anion site, which then becomes charge neutral. This leaves a charge imbalance in the surface; the cations surrounding the now neutralized anion site create a locally positive region on the surface (Fig. 1(b)). It is the

Coulomb attraction between this positive patch on the surface and the negatively charged scattering atom, that leads to the downshift required to bring the electron affinity and the valence band into resonance,[10,11] as depicted in Fig. 1(b).

A model of these charge-transfer reactions has been developed by Borisov and Sidis[10,11] based on a binary collision formalism with a diabatic description of the energetics.[12] They obtained coupled time-dependent equations for the amplitudes in the two diabatic configurations, generating the time-dependence with classical trajectories, although the motions normal to and parallel to the surface were decoupled and treated separately. For F/LiF, their diabatic potentials representing the F^0 and F^- configurations do not cross. A threshold energy is thus required for negative-ion production, but above this the ions are formed with unit probability. For F/KI there is a curve-crossing and, in consequence, a lower threshold energy. This is in broad agreement with experimental results in the lower part of the energy range considered (below $\sim$20 keV), while above this, the negative-ion fraction decreases steadily to zero.

In this paper we consider a similar model of the negative-ion formation. We use diabatic potential energy surfaces (PESs), generated by a semi-empirical procedure, however, we treat the motion of the projectile in a fully quantum fashion allowing full coupling between the normal and parallel motions. We find that in our model, the ion-formation probability is unity at all energies considered, however, we obtain a threshold for the detection due to trapping of the ions at the lowest energies. In the following section, we review the semiempirical scheme used to generate the PESs. Following this, we present some details of the quantum wavepacket calculations that are necessary to deal with the unusually high energies (at least for wavepacket methods) considered in this problem. We then discuss our results and conclusions.

II. The diabatic PESs

A. General considerations

In this work, we employ a diabatic description; the electronic states are not eigenstates of the Hamiltonian for fixed nuclear positions, $\boldsymbol{R}$, rather we use basis functions which are products of atomic-like orbitals centred on the atom positions. Specifically, for each electronic configuration we use a single Slater determinant. For example, for the ground-state (GS) electronic wavefunction, describing neutral ionic surface and neutral atom, we write

$$\chi_{\mathrm{gs}} = \det\left\{\left[\prod_k X_k \bar{X}_k\right] A\right\}. \tag{1}$$

Here, X_k, $\bar{X}_k$ and A are spin eigenfunctions for the valence electrons (we have omitted explicit reference to the core electrons) sited on the halide (X) or projectile (A) sites. For the crystal, this assumes that the valence electrons are fully localized on the anion sites, *i.e.* the anion and cation sites have integer multiples of charge. There is essentially no band-structure; the valence band is a δ-function. This is a reasonable approximation for the alkali-metal halide surfaces examined in the present paper.[13–15] Similarly, we write for the excited state wavefunction formed when charge is transferred from a halide site to the projectile atom (which we shall call the negative ion state or NIS)

$$\chi_{\mathrm{A}-} = \det\left\{\left[\prod_{k=1}^{N-1} X_k \bar{X}_k\right] X_{\mathrm{N}} A \bar{A}\right\}. \tag{2}$$

In standard fashion, we can employ these electronic orbitals to obtain a matrix equation for the time dependence of the nuclear wavefunction. With a general Hamiltonian of the form

$$\mathscr{H} = \hat{K}_{\mathrm{n}} + \hat{K}_{\mathrm{e}} + v_{\mathrm{n}} + v_{\mathrm{e}} + v_{\mathrm{n-e}}, \tag{3}$$

where $\hat{K}_{\mathrm{n}}$ ($\hat{K}_{\mathrm{e}}$) is the kinetic energy operating on the nuclear (electronic) coordinates, v_{n} (v_{e}) is the internuclear (interelectronic) Coulomb repulsion and $v_{\mathrm{n-e}}$ is the electron–nuclei interaction, the time-dependent Schrödinger equation for the nuclear motion becomes (ignoring the derivatives of electronic wavefunction with respect to nuclear coordinate)

$$\mathrm{i}\frac{\partial \psi_\nu(\boldsymbol{R})}{\partial t} = (\hat{K}_{\mathrm{n}} + v_{\mathrm{n}} + \langle \chi_\nu | K_{\mathrm{e}} + v_{\mathrm{e}} + v_{\mathrm{n-e}} | \chi_\nu \rangle)\psi_\nu + \sum_\mu \langle \chi_\nu | K_{\mathrm{e}} + v_{\mathrm{e}} + v_{\mathrm{n-e}} | \chi_\mu \rangle \psi_\mu, \tag{4}$$

where ψ_v is the nuclear wavefunction corresponding to electronic configuration, v. We can write this more simply as a matrix equation for vector Ψ

$$\mathrm{i}\,\frac{\partial \Psi(\boldsymbol{R})}{\partial t} = (\boldsymbol{K} + \boldsymbol{V})\Psi, \tag{5}$$

where $\boldsymbol{K}$ is a diagonal matrix given by $\boldsymbol{K} = \mathrm{diag}\,(\hat{K}_n)$, and $\boldsymbol{V}$ is a potential energy matrix. Each electronic configuration, represented by one of the X_v, generates a separate PES forming the diagonal elements of $\boldsymbol{V}$. The off-diagonal elements give the couplings between the different configurations, and induce charge transfer or changes in bonding.

Charge can, of course, be transferred at any halide site, and so there is a NIS PES for every halide site on the surface. Therefore, even when we consider only the GS and NISs, the potential matrix and wavefunction vector are infinite in size, with an NIS matrix element centered on each and every halide site

$$\boldsymbol{V} = \begin{pmatrix} V_{11} & V_{12} & V_{13} & \cdots \\ V_{12} & V_{22} & V_{23} & \\ V_{13} & V_{23} & V_{33} & \\ \vdots & & & \ddots \end{pmatrix}, \tag{6}$$

where V_{11} is the GS PES generated using the wavefunction of eqn. (1). The diagonal elements V_{22}, V_{33}, *etc*., describe the interaction between a negative ion and the surface with one neutral halogen site, while the off-diagonal elements in the first row and first column, V_{12}, V_{13}, *etc*., couple these excited states to the electronic GS, *i.e*., they induce the electron transfer. Fortunately, because of the surface periodicity, the NIS matrix elements are related to one another simply by shifts of whole numbers of lattice vectors, and so need only be computed for one site. The other off-diagonal elements, V_{23}, V_{35}, *etc*., couple the excitations at different sites; they describe the hopping of electrons (or holes) between the halogens. Although these are non-zero in the Slater orbital basis employed here, they are negligibly small.

B. Computation of the PES matrix elements

To make an explicit computation of the elements of $\boldsymbol{V}$, we use a semi-empirical valence bond (SEVB) method developed for gas-phase studies of alkali-metal halide PESs and dynamics.[16–18] This has been extended previously to deal with the case of ions bonding to metal halide surfaces.[19] The basis of this approach is to factor the Hamiltonian (excluding the nuclear kinetic energy) into diatomic-like terms in a fashion similar to the diatomics-in-molecules method[20] used in gas-phase dynamics,

$$H = \sum_p H_p + \sum_p \sum_{q<p} V_{pq} \tag{7}$$

where p and q label the atomic sites. H_p is a 'single atom' Hamiltonian given by (using atomic units)

$$H_p = \sum_{i=1}^{n(p)} \left\{ -\frac{1}{2m}\nabla_i^2 - \frac{Z_p}{|r_i - R_p|} \right\} + \sum_{i=1}^{n(p)} \sum_{j<i} \frac{1}{r_{ij}} \tag{8}$$

where i, j label the $n(p)$ electrons on atom p, which has nuclear charge Z_p, m is the mass of the electron and the r_i (R_p) are the electron (nuclear) positions. The first approximation in the SEVB method is to separate this into core and valence electrons, and assume the cores are localized at the nucleus. We can then replace the core terms in eqn. (8) by an energy that is independent of the valence configuration. By choice of energy zero, these core energies can actually be omitted. Additionally, the core electrons act to screen the nuclear charge. In the examples considered in this paper, the effective nuclear charge is reduced to $+1$. Thus eqn. (8) becomes

$$H_p = \sum_{i=1}^{n_v} \left\{ -\frac{1}{2m}\nabla_i^2 - \frac{1}{|r_i - R_p|} + \sum_{j<i} \frac{1}{r_{ij}} \right\} \tag{9}$$

where n_v is the number of valence electrons. In the following we shall always take this to be 0, 1 or 2, corresponding to a singly charged positive ion, a neutral atom and a singly charged negative ion, respectively. With these approximations, the interaction term V_{pq} is given by

$$V_{pq} = -\sum_{i=1}^{n_v(p)} \frac{1}{|r_i - R_q|} - \sum_{j=1}^{n_v(q)} \frac{1}{|r_j - R_p|} + \sum_{i=1}^{n_v(p)} \sum_{j=1}^{n_v(q)} \frac{1}{r_{ij}} + \frac{1}{R_{pq}} + V_{cc}(p, q) \tag{10}$$

The first two terms in this give the attraction between the core of one atom and the electrons of the other, the second term is the repulsion between electrons on different atoms, and the third term is the nuclear–nuclear repulsion. The final term in eqn. (10) is due to the interaction of the cores with each other and to the core–valence interaction.

Combining eqns. (9) and (10) with the electronic wavefunctions of eqn. (1) and (2) gives us the elements of $\boldsymbol{V}$ in eqn. (6). The GS is given by

$$V_{11} = \langle \chi_{gs} | H | \chi_{gs} \rangle. \tag{11}$$

Similarly, the NIS elements are given by

$$V_{22} = \langle \chi_{A^-} | H | \chi_{A^-} \rangle. \tag{12}$$

The partitioning of the electrons into those on atom p and those on atom q is arbitrary. In calculating V_{11} and V_{22} we actually divide the electrons differently: for V_{22} we 'move' one electron from a halide site onto A. We do not, however, explicitly compute any of the integrals in eqns. (11) and (12), rather at this point we introduce the empirical part of the SEVB method, evaluating the integrals by the point-charge approximations.[21] For example,

$$\langle \mathrm{A} | H_{\mathrm{A}} | \mathrm{A} \rangle = -E_i(\mathrm{A}), \tag{13}$$

$$\langle \bar{X}_i X_i | H_{X_i^-} | \bar{X}_i X_i \rangle = -E_i(\mathrm{X}) - E_{ea}(\mathrm{X}) \tag{14}$$

and

$$\langle \bar{X}_i X_i \bar{A}A | H_{X_i^- A^-} | \bar{X}_i X_i \bar{A}A \rangle = V_{cc}(\mathrm{X}_i, \mathrm{A}) + \frac{1}{R_{AX_i}}, \tag{15}$$

where E_i and E_{ea} are the ionization potential and electron affinity, respectively. We neglect all three-centre integrals and higher.

The only remaining unknown in this scheme is the 'core–core repulsion' term, V_{cc}. In the form we have partitioned the Hamiltonian, this is a purely diatomic property, we have a different V_{cc} for each pair of atom types. It is an assumption of the SEVB method that these core–core terms are transferrable to all environments in which the atom-pair finds itself. As in previous work,[16] we repeat the algebra above, deriving a PES matrix for the ground and excited states of the diatomic alone. The eigenvalues of this are then fit to the known binding energy curve, which after some algebraic rearrangement yields V_{cc}. Further details of this may be found in ref. 16 and 22. By construction, the SEVB method gives the exact binding energy curve for the diatomic molecule, V_{cc} is the correction which makes this so. Although we call it the core–core repulsion, it is not purely repulsive, but rather has a shallow well some 10 s of eV deep. To have a convenient functional form for later work, we fit V_{cc} to a sum of Gaussians.

Combining all of the above, and by choosing the energy zero to be the energy of the neutral atom and neutral surface at infinite separation, the GS potential for the atom–surface interaction is

$$V_{11} = \sum_p \{V_{cc}(\mathrm{A}, \mathrm{X}_p) + V_{cc}(\mathrm{A}, \mathrm{M}_p)\}, \tag{16}$$

where M_p are the cations (metal ions). This is predominantly repulsive, but has a very shallow chemisorption well. We add to this a component accounting for the dipole induced on A by the surface charges, which does not arise in the SEVB scheme. The form of this is discussed below.

The induced-dipole terms are more important for the NIS, where we must account for the polarization of the A^- by the surface and for the polarization of the surface by the A^-. The

polarizations of the crystal atoms also change when one halide site is neutralized, giving

$$V_{22} = E_{\mathrm{i}}(\mathrm{X}) - E_{\mathrm{ea}}(\mathrm{A}) + E_{\mathrm{mad}} + \Delta V_{\mathrm{xpol}} + \sum_p \{V_{\mathrm{cc}}(\mathrm{A}, \mathrm{X}_p) + V_{\mathrm{cc}}(\mathrm{A}, \mathrm{M}_p)\}$$
$$+ \sum_p \left\{\frac{1}{R_{\mathrm{AX}_p}} - \frac{1}{R_{\mathrm{AM}_p}}\right\} - \frac{1}{R_{\mathrm{AX}_N}} + V_{\mathrm{dip}}(\mathrm{A}^-)$$
$$- \sum_p \left\{\frac{\alpha(\mathrm{X}^-)}{R^4_{\mathrm{AX}_p}} + \frac{\alpha(\mathrm{M}^+)}{R^4_{\mathrm{AX}_p}}\right\} + \frac{1}{2R^4_{\mathrm{AX}_N}} \{\alpha(\mathrm{X}^-) - \alpha(\mathrm{X})\}, \tag{17}$$

where E_{mad} is the Madelung energy of the crystal, ΔV_{xpol} the change in the polarization energy of the crystal and the αs are the polarizabilities of the respective ions and atoms. The change in crystal polarization is not easy to obtain, however the potential is constructed semi-empirically, so it makes perfect sense to replace the first four terms by the known asymptotic value of the potential, *i.e.* by $\Phi - E_{\mathrm{ea}}(\mathrm{A})$, the energy required to move an electron from the surface to infinity (the work function Φ) and then to deposit it onto A ($-E_{\mathrm{ea}}(\mathrm{A})$). The eighth term is the energy of the dipole induced on the A^- ion by the crystal pointcharges, which has basically the same form as the correction for the GS. The final two terms describe the polarization of the crystal by the A^- ion. Clearly these are treated as diatomic-like again, *i.e.* we have neglected any screening of the induced dipoles by the surrounding crystal. This term will therefore be an overestimate of the true induced-dipole energies.

Finally we write

$$V_{22} = \Phi - E_{\mathrm{ea}}(\mathrm{A}) + V_{11} + V_{\mathrm{pc}} + V_{\mathrm{dip}}(\mathrm{A}^-) + V_{\mathrm{pol}}, \tag{18}$$

where V_{pol} represents all the ion induced crystal polarization terms.

$$V_{\mathrm{pc}} = \sum_p \left\{\frac{1}{R_{\mathrm{AX}_p}} - \frac{1}{R_{\mathrm{AM}_p}}\right\} - \frac{1}{R_{\mathrm{AX}_N}} \tag{19}$$

is the interaction of A^- with all the point charges in the surface. The sum is taken over all surface sites (so that we may express this as a Fourier series, as discussed below), and so we must explicitly account for the neutral atom at the site labelled X_N. The $1/R$ Coulomb attraction into the locally positive, active halide site is especially clear in eqn. (19).

For consistency with the determination of V_{cc} we have also included in the diagonal matrix elements the terms proportional to $S^2_{\mathrm{AX}} = |\langle X|A\rangle|^2$. These are, however, small compared to the other terms, so we omit discussion of them here.

The greatest advantage of the SEVB method is that we can obtain the off-diagonal matrix elements within the same scheme and with the same approximations used for the diagonal matrix elements. The coupling between V_{11} and V_{22} is

$$V_{12} = \tfrac{1}{2} S_{\mathrm{AX}_N} \left\{V_{11} + V_{22} - V_{\mathrm{pc}} + E_{\mathrm{mad}} - \tfrac{1}{2}(\rho_{\mathrm{A}} + \rho_{\mathrm{X}}) + \frac{1}{R_{\mathrm{AX}_N}}\right\}, \tag{20}$$

where ρ_{A} and ρ_{X} are the screening constants of the outer electrons of A and X.[23] Analytic approximations for the overlap integral $S_{\mathrm{AX}_N} = \langle X|A\rangle$ have been given by Mulliken *et al.*[24]

C. Fourier expressions for lattice summations

To evaluate the summations over lattice positions, we employ Fourier expansions, checked by explicit summation over finite clusters. In the following, we assume the crystal has a square NaCl type lattice. As detailed by Steele[25] we split the summations into those over atoms in identical positions, *i.e.* we sum anion and cation sites separately, and odd and even planes separately.

$$\sum_p V_{\mathrm{cc}}(\mathrm{A}, \mathrm{X}_p) = \sum_p \sum_n B_n \exp(-\alpha_n R^2_{\mathrm{AX}_p}) = F^{\mathrm{even}}_{\mathrm{cc}} + F^{\mathrm{odd}}_{\mathrm{cc}} \tag{21}$$

where

$$F^{\mathrm{even}}_{\mathrm{cc}} = \sum_{g_1 g_2} \sum_n \sum_k \frac{\pi B_n}{a_{\mathrm{s}} \alpha_n} \mathrm{e}^{-\alpha_n z_k^2} \mathrm{e}^{-g^2/4\alpha_n} C_1(g_1, g_2, x, y) \tag{22}$$

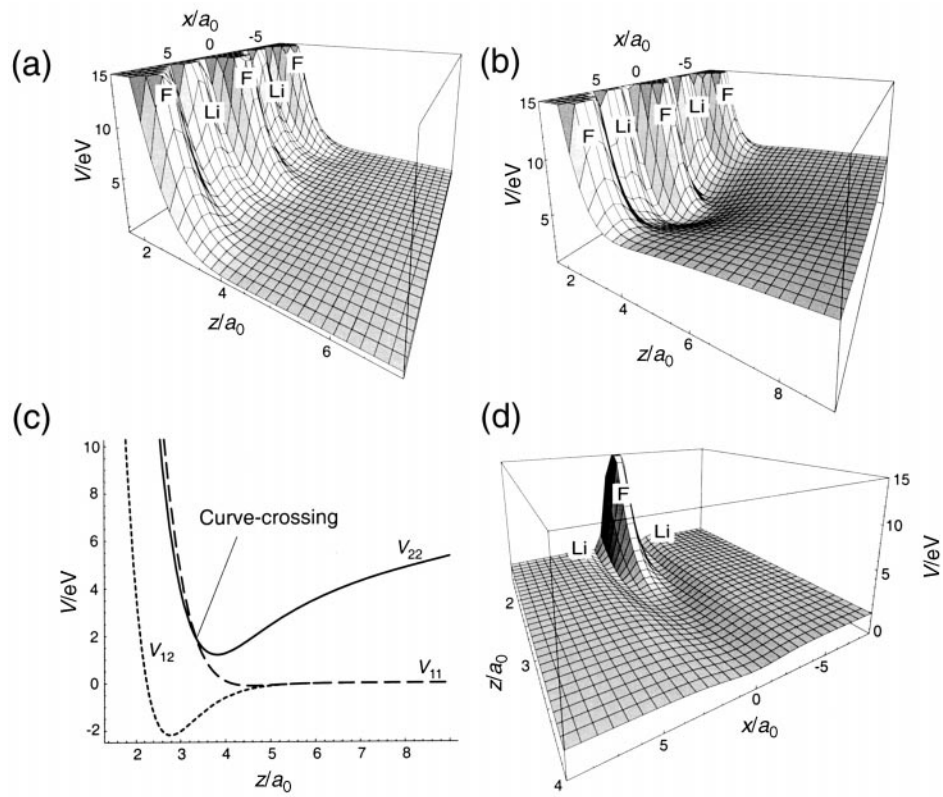

Fig. 2 The SEVB PESs for the F/LiF(100) system. (a) The ground-state PES representing the interaction of neutral surface with neutral atom. The cut shown runs along the tops of the surface atoms in the ⟨010⟩ direction. The spacing between alkali-metal and halide sites is 3.81 a_0. (b) The negative-ion state PES representing the interaction of an F^- ion with an LiF surface with one neutralized F site (located at the origin). The coordinates are the same as for panel (a). (c) The PESs as a function of distance above the site of charge transfer. (d) The off-diagonal coupling, *i.e.* V_{12}, between the ground and NIS states.

where g_1 and g_2 are reciprocal lattice vectors, $g = |g_1 + g_2|$, k sums over even planes only, a_s is the area of the unit cell, x and y are coordinates in the surface plane and z_k is the vertical distance to the kth plane, and

$$C_1(g_1, g_2, x, y) = \cos(g_1 x)\cos(g_2 y)\{1 + (-1)^{G_1+G_2}\}2^{2-\delta_{0,G_1}-\delta_{0,G_2}} \tag{23}$$

with $g_1 = 2\pi G_1/a_x$ where a_x is the lattice constant. For the odd planes, we obtain an identical expression, but with C_1 replaced by

$$C_2(g_1, g_2, x, y) = \cos(g_1 x)\cos(g_2 y)\{(-1)^{G_1} + (-1)^{G_2}\}2^{2-\delta_{0,G_1}-\delta_{0,G_2}}, \tag{24}$$

and for the summations over M-sites we simply exchange C_1 and C_2. Similarly we can get

$$V_{pc} = \frac{32\pi}{a_s} \sum_{g_1 g_2}{}' \frac{e^{-gz} \cos g_1 x \cos g_2 y}{g(1 + \exp(-g a_x/2))}, \tag{25}$$

where the prime indicates summation over odd reciprocal lattice vectors only. The polarization term, V_{pol} also splits into separate summations for M and X atoms differing only by the symmetry factors C_1 and C_2. For the X sites we get

$$V_{pol}(X) = \frac{-\pi\alpha(X^-)}{2a_s} \sum_{g_1 g_2} \sum_k \left\{ \frac{g}{z_{2k}} K_1(g z_{2k}) C_1 + \frac{g}{z_{2k+1}} K_1(g z_{2k+1}) C_2 \right\}, \tag{26}$$

where K_1 is a modified Bessel function of the second kind. Finally,[25]

$$V_{\mathrm{dip}}(\mathrm{A}) = -\frac{1}{2}\,\alpha(\mathrm{A})\,\frac{256\pi^2}{a_s^2}\left\{\frac{\exp(-4\pi z\sqrt{2}/a_x)}{(1+\exp-\pi\sqrt{2})^2}\right\}\left\{2+\cos\frac{4\pi x}{a_x}+\cos\frac{4\pi y}{a_x}\right\}, \tag{27}$$

where the lattice constant, a_x, is the same in both directions, x and y.

The end result of this lengthy, but largely straightforward, manipulation, is shown in Fig. 2 for the F/LiF(100) system. The GS PES, panel (a), is predominantly repulsive, more so at the halide than at the alkali-metal sites, and is perfectly periodic. The NIS PES in contrast, is not periodic because of the $1/R$ attraction from the active site, located at the origin of the coordinates. Moving away from this site, however, the halide and alkali-metal sites are in turn repulsive and attractive to the A^- ion. Asymptotically, V_{22} lies $\Phi - E_{\mathrm{ea}}(\mathrm{A})$ above V_{11}. The Coulomb attraction serves to decrease this energy gap. For F/LiF(100), we actually get a curve-crossing between the PESs at $z \sim 3.35\ a_0$, as can be seen in panel (c). This is in contrast to Borisov and Sidis[11] who found no curve-crossing for this system. The influence of the curve-crossing on the subsequent ion formation probability remains to be fully ascertained. As can be seen from panel (d), the off-diagonal matrix element is only significant at the active site.

III. Wavepacket propagation

To follow the quantum motion of the projectile atom, we have used time-dependent wavepacket methods with fast Fourier transforms (FFTs) to switch between real and momentum space to apply, in turn, the potential and kinetic energy operators. The use of FFTs imposes restrictions on the finite element grids on which the nuclear wavefunction and operators are represented. Firstly, the grid is periodic. In the z-direction, we must remove the wavepacket from the end of the grid, which we do by grid-cutting.[26] Parallel to the surface, we must ensure that the negative ion cannot return and re-interact with the active site, and become a neutral again, so the grid must be sufficiently long that when the ion returns, it does so at large z where V_{12} is negligible. Secondly, however, the lengths of the momentum and real space grids are linked since the maximum momentum, $K_{\mathrm{max}} = N\pi/L$, where L is the length of the real-space grid, and N the number of grid points. At the grazing incidence conditions of the experiment, the momentum parallel to the surface is very high. To accommodate large L with large K_{max} we employ the shift-theorem of Fourier transforms to centre the momentum at a high value, K_0:[27] before the FFT to momentum space, we multiply the wavefunction by the shift factor $\mathrm{e}^{-\mathrm{i}K_0 x}$ and after determining the kinetic energy and FFTing back to real space, we shift back with the factor $\mathrm{e}^{+\mathrm{i}K_0 x}$. We also reduce the momentum-space grid by employing a projectile mass of 1 u rather than 19 u. As shown below, this makes little difference to the results.

As noted above, to an incoming particle, all surface sites appear equivalent; ion formation can occur at any. The GS PES and wavefunction are therefore periodic. The NIS PES is not periodic because a charge defect is left at the active halide site, this site thus appears different from the remainder of the surface (Fig. 2(b)). A separate NIS PES is required for each site, therefore a separate NIS wavefunction is also required for every halide site. As for the PES, however, the NIS wavefunctions are identical up to a shift of a lattice vector parallel to the surface. Consider a halide site, labelled 2, centred at $x = 0$; the equation-of-motion for the NIS state, ψ_2, is

$$\mathrm{i}\,\frac{\partial\psi_2(x,y,z,t)}{\partial t} = (\hat{K}_n + V_{22}(x,y,z))\psi_2(x,y,z,t) + V_{12}(x,y,z)\psi_1(x,y,z,t). \tag{28}$$

Similarly, if ψ_3 represents the excitation at a halide site one lattice constant away, it obeys the same equation-of-motion with the label 3 replacing 2. But, $\psi_3(x, y, z, t) = \psi_2(x - a_x, y, z, t)$, $V_{33}(x, y, z) = V_{22}(x - a_x, y, z)$ and $V_{13}(x, y, z) = V_{12}(x - a_x, y, z)$. As the GS wavefunction, ψ_1, is always periodic, so the equation-of-motion for ψ_3 becomes

$$\begin{aligned}\mathrm{i}\,\frac{\partial\psi_2(x-a_x,y,z,t)}{\partial t} &= (\hat{K}_n + V_{22}(x-a_x,y,z))\psi_2(x-a_x,y,z,t)\\ &\quad + V_{12}(x-a_x,y,z)\psi_1(x-a_x,y,z,t),\end{aligned} \tag{29}$$

i.e., the same as eqn. (28) but with a coordinate shift. The equation-of-motion for the GS

$$i\frac{\partial\psi_1(x,y,z,t)}{\partial t} = (\hat{K}_n + V_{11}(x,y,z))\psi_1(x,y,z,t) + V_{12}(x,y,z)\psi_2(x,y,z,t) + V_{13}(x,y,z)\psi_3(x,y,z,t) + V_{14}(x,y,z)\psi_4(x,y,z,t) + \cdots \quad (30)$$

becomes

$$i\frac{\partial\psi_1(x,y,z,t)}{\partial t} = (\hat{K}_n + V_{11}(x,y,z))\psi_1(x,y,z,t) + V_{12}(x,y,z)\psi_2(x,y,z,t) + V_{12}(x-a_x,y,z)\psi_2(x-a_x,y,z,t) + V_{12}(x-2a_x,y,z)\psi_2(x-2a_x,y,z,t) + \cdots \quad (31)$$

Clearly then, ψ_2 and V_{22} can perform the role of all of the excited states if we simply add the off-diagonal contribution (shifted appropriately in x) to ψ_1 many times over.

The explicit time-dependence of the wavefunction is solved using the Chebychev method[28]

$$\Psi(t+\Delta t) = e^{-iH\,\Delta t}\Psi(t) = \sum_n a_n(t)T_n(\tilde{H})\Psi(t). \quad (32)$$

The Chebychev polynomials, T_n, calculated recursively, are functions of the Hamiltonian, renormalized to have eigenfunctions in the range $[-1, 1]$. Care must be taken when renormalizing H because although only two NISs are stored, there are effectively very many (>50) and so H has a much larger spectral range than might be expected. In common with all other Chebychev implimentations, we limit the eigenvalues of H by imposing a cut-off on the potential (values of 50–100 eV seem adequate), and also by saturating the parallel momentum contribution to the kinetic energy operator when it is >50 eV from $K_0^2/2M$.[29]

A general approximation in models of grazing incidence scattering from surfaces is to limit the dimensionality in that the projectile can only move in a plane perpendicular to the surface, parallel to the incident beam direction, *i.e.* the calculations are performed on a two-dimensional slice corresponding to the PESs shown in Fig. 2. The initial wavefunction is taken to be the product of a plane-wave state in x (running in the $\langle 010\rangle$ direction) with a Gaussian-weighted plane-wave in z. Grid lengths of 240×240 points are used at the lower energies, increasing to 480×240 at higher energies.

IV. Results and discussion

A. The threshold region

Fig. 3 shows a snapshot of the wavepacket on the two surfaces part way through a scattering event, for an initial translational energy of 4 keV at an incidence angle of 1° relative to the surface plane (the "normal energy", $\varepsilon_i \cos^2\theta = 1.22$ eV in this case). The ground-state wavefunction, shown in Fig. 3(a), is periodic in x (actually it appears structureless at these incidence conditions). On the GS, it never quite reaches the crossing point (which becomes a line, or seam, in two dimensions) as it has insufficient normal energy (the crossing is at an energy of 1.98 eV at the active site). Instead, it can be seen to transfer efficiently onto the NIS PES, as in Fig. 3(b), which shows the NIS for the halide site at $x = 0$. The transfer appears to be very strongly localised on the active site, the wavefunction streaming rapidly away from a region just before the highest point of the crossing seam, *i.e.* from the classical turning point on the GS PES. Transforming the wavefunctions and PESs to an adiabatic representation gives a clearer picture of the local nature of the charge exchange. We can see from the lower two frames of Fig. 3 that the wavepacket jumps diabatically from the lower adiabatic state (Fig. 3(c)) to the upper adiabatic state (Fig. 3(d)) in the turning region (smeared out in quantum mechanics because of the tunneling into the repulsive wall). (Note that the adiabatic transformation is strictly only valid in the neighbourhood of $x = 0$ because we have not transformed with the full PES and wavefunction, having NIS elements at every halide site, but only with the NIS state at the origin.)

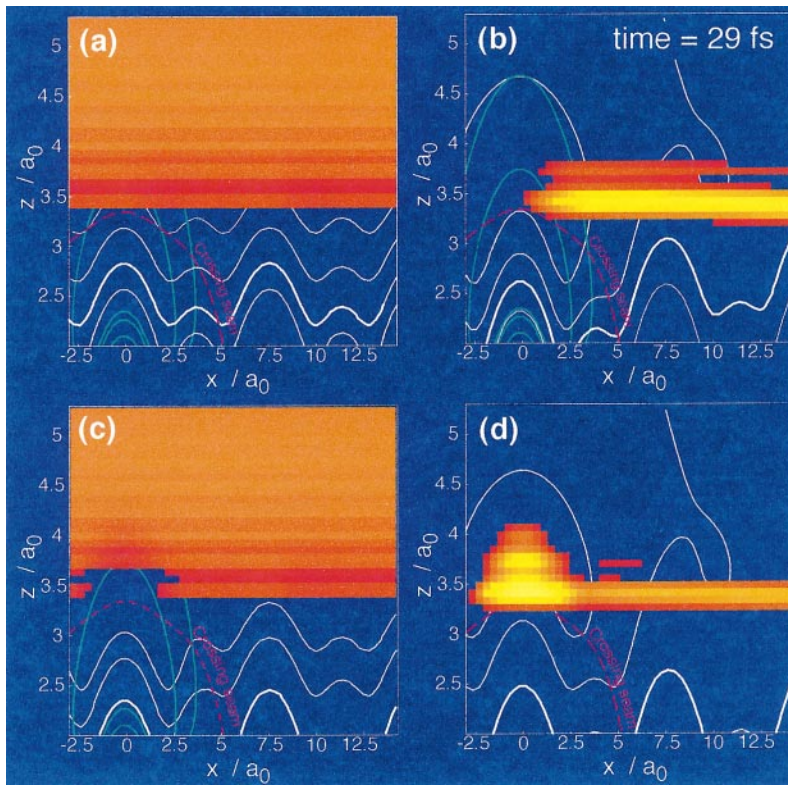

Fig. 3 (a) The wavefunction on the ground-state PES incident at 4 keV at an angle of 1° to the surface plane, with normal energy of 1.22 eV. The white lines show a contour plot of the PES, the green lines are a contour plot of the V_{12} matrix element, and the purple line shows the locus of points where V_{11} and V_{22} cross. The wavepacket intensity decreases from white, though yellow to red, with the very lowest values removed for clarity. (b) The wavefunction on the NIS located on the halide site at the origin. The white lines now show a contour plot of V_{22}. The transfer between states clearly occurs on the active site, just before the curve crossing. (c) and (d) The wavepacket from (a) and (b) transformed into an adiabatic representation, with corresponding adiabatic PES shown as white contour lines. The charge transfer occurs diabatically at the active site, as evidenced by the sudden jump from (c) to (d) at $x = 0\ a_0$, $z \sim 3.5\ a_0$.

Following the wavepacket in time, we find that the intensity on the GS gradually disappears, transferring onto the NISs. In other words, the incoming atoms convert, almost entirely, to negative ions, as can can be seen in Fig. 4, which shows the integrated intensities on the GS and NISs (summed over all halide sites) for the same incidence conditions as Fig. 3. Quite clearly, the intensity on the NIS increases smoothly at the expense of that on the GS, *i.e.*, *the probability of forming a negative ion in the initial collision*, P_i, *is approximately 1*. We have found this to be so across the entire energy range considered here (1 eV–15 keV) for both the F/LiF(100) and F/KI(100) systems. The intensity does not return to the GS at the active site because the newly formed negative ions move very rapidly away from there in the x-direction, passing out the side of the region of strong coupling.

To follow the evolution of the NIS wavefunction with minimum disturbance from periodic return to the active site, we stop the full propagation once the transfer to the NIS state is complete, and then propagate the wavefunction on this state alone, with the origin displaced far from the active site. Long propagation times are then possible, as can be seen in Fig. 4. The intensity on the NIS state is stable up until $\sim$100 fs when there is a slight decline. This is due to the grid-cutting in the z-direction which removes wavepacket intensity before the end of the grid. The remainder of the wavepacket fails to reach the end of the grid. It has failed to acquire the full 8.58

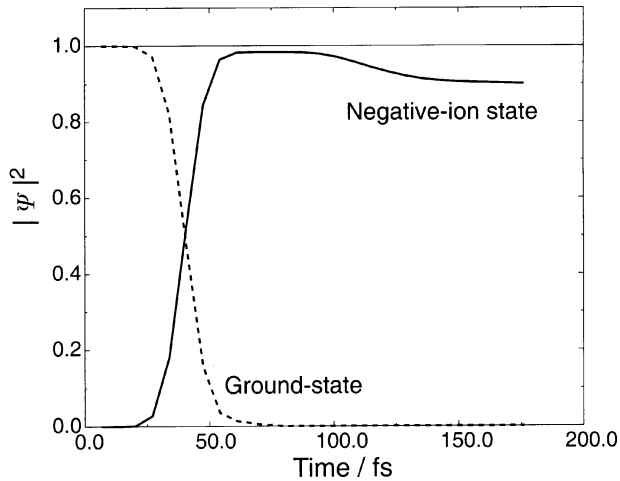

Fig. 4 The total normalization of the wavepackets on the ground and negative-ion states *vs.* simulation time for an initial energy of 4 keV incident 1° from the surface plane. After ~25 fs, the incoming neutral atoms gradually convert, almost entirely, to negative ions. After ~100 fs, some ions have escaped from the surface (the wavepacket is cut from the edge of the grid causing the decrease in normalization), but almost 90% remain trapped.

eV of normal energy required to escape the surface and remains trapped in the weak attraction of the polarization and point-charge contributions to the PES. In other words, for these incidence conditions, only ~10% of the incident atoms escape the surface as negative ions *in the first bounce*, although there is initially 100% conversion to negative ions.

Clearly, the initial ion-formation probability, P_i, is a poor approximation to the experimental results for the F/LiF(100) system, lacking as it does any threshold. However, we do obtain a threshold if we count only those negative ions escaping the surface in the first bounce. This effective negative ion fraction, P_N, is shown in Fig. 5, top panel, for the F/LiF(100) system. The threshold we obtain is very close to that in experiment, and shifts to lower energy as the angle of incidence is increased because there is then more normal energy to aid escape from the surface. It can also be seen from Fig. 5, top panel, that for this system, averaging the results over several impact planes, *i.e.* averaging over the y-coordinate not explicitly treated in the dynamics, has little effect on the results.

The normal energy corresponding to the threshold region is far below that required by the NIS asymptotically; even at 14 keV, the normal energy at 1° incidence angle is only 4.36 eV, compared to the 8.58 eV separation of V_{11} and V_{22} in the F/LiF system. The extra energy comes from the very high parallel motion, in quite straightforward fashion. As can be seen in Fig. 3, the wavepacket on the upper state leaves the active site travelling predominantly in the x-direction. When it reaches $x = 7.62\ a_0$, it encounters the next halide site along from the active site, and experiences a strong Coulomb repulsion of like charges. In other words, it moves uphill away from the active site, using up parallel momentum to do so. Some of the potential energy gained in doing this (if we assume the negative ion moves horizontally away from the curve-crossing it encounters a potential of ~6 eV at the next halide site along) is channelled into normal motion, thereby reducing the normal energy escape threshold. The ultimate fate of the trapped ions is difficult to determine in the present model. We assume that the energy is much too high for permanent trapping and that on return to the surface, the ions re-neutralize (which costs more energy) and return to the gas phase after the second bounce. This remains to be fully tested.

The escape probability of the negative ion can also be enhanced by reducing the energy required asymptotically for the NIS. This can be done by changing to a surface with a lower workfunction, such as the KI(100) surface. As shown in the lower panel of Fig. 5, the threshold in P_N for F/KI(100) occurs at much lower incident energies, in agreement with experiment.[4] Once again, this threshold arises solely from the trapping behaviour, P_i is always close to unity. In the present model, the shift in threshold is due solely to the smaller workfunction—the PESs for

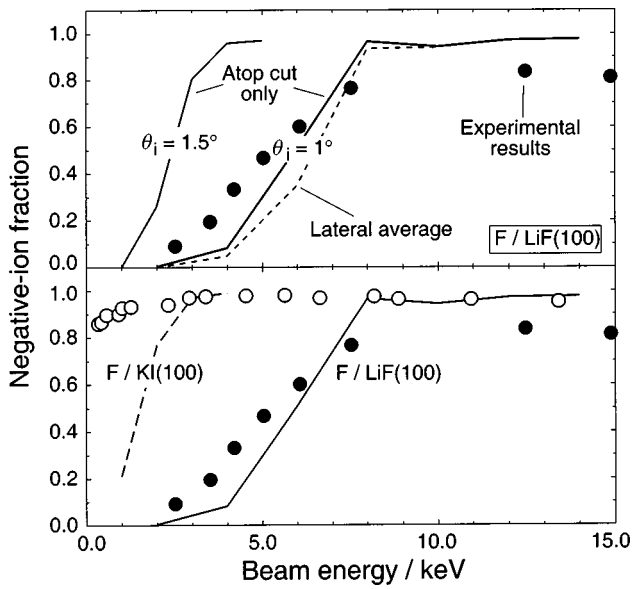

Fig. 5 Top panel: Negative-ion fraction *vs.* incident energy obtained by counting only the promptly scattered ions (i.e. excluding the trapped fraction) for the F/LiF(100) system. In all cases, the initial ion formation probability is high. The atop cut runs across the surface atoms in the ⟨010⟩ direction (*cf.* Fig. 2). Motion is restricted to a plane. Averaging over several such planes in the ⟨010⟩ direction clearly makes little difference to the results. The threshold energy decreases with initial angle because the increase in normal energy makes escape more likely. Experimental results are shown as filled circles. Bottom panel: Negative-ion fraction *vs.* incident energy for F scattering from LiF(100) and KI(100) at an incident angle of 1°. Trapped ions are not counted, and results are for the atop slice only. Experimental results are indicated by filled/open circles for LiF/KI.

F/LiF and F/KI do not differ greatly, except that for the latter system, there is no translational threshold to reach the curve-crossing point. In general, from this trapping model, we predict that the lowest energy *thresholds* will occur for atoms with high electron affinities incident on surfaces with low workfunctions, as this yields the smallest asymptotic separation between ground and excited states.

B. Re-neutralization at the surface

The final yield of negative ions will also be determined by the re-neutralization (RN) probability. There are two possible mechanisms for this: charge transfer into the conduction band of the solid, and electron emission into the gas phase.[30] To explore the influence of RN on the threshold behaviour, we have included the former process, charge transfer from the projectile back to the surface, although the latter can also be expected to be important, especially for LiF, which has a negative electron affinity. We incorporate RN into the present model by adding another diabatic state to represent electron transfer into the conduction band of the solid. Again, we assume that this is a purely local event, occurring this time into an atomic-like orbital on one of the alkali-metal sites. The extra diagonal and off-diagonal PES matrix elements are generated using the electron wavefunction

$$\chi_{\mathrm{RN}} = \det\left\{\left[\prod_{k=1}^{N-1} X_k \bar{X}_k\right] X_N M_L \bar{A}\right\}. \tag{33}$$

The diagonal PES for RN is basically identical to the GS PES, but shifted up by the band-gap energy, E_{gap} of the crystal

$$V_{\mathrm{RN}} = E_{\mathrm{gap}} + V_{11} - \left(\frac{1}{R_{\mathrm{X}_N \mathrm{M}_P}} - \frac{2}{a_x}\right), \tag{34}$$

where the last term accounts for the reduction in the Madelung energy cost when the ion-formation and re-neutralization sites are near one another.

The NIS wavefunction is not periodic, so the alkali-metal sites are not all equivalent in this process. To approximate the effect of interacting with many alkali-metal sites, we compute the RN for each in a separate calculation, assuming it is the only RN site and use recursion to compute the net survival probability, S, of the negative-ion

$$S = \lim_{n\to\infty} [1 - P_{\mathrm{RN}}(n)]S(n), \tag{35}$$

where $P_{\mathrm{RN}}(n)$ is the probability of RN at site n, and $S(n)$ is the probability that the negative ion has survived re-neutralization at all sites before n. The implicit assumption here is that the fraction not re-neutralizing is unaffected by V_{RN}.

Since another charge defect is created in the surface, RN requires additional energy to be taken from the projectile motion, *i.e.* the PES lies above the NIS PES at large z. There is no crossing between the NIS and RN PESs, so transfer is by a near-resonant Demkov-type process.[31] At the lowest energies, there is simply not enough normal energy, RN does not occur and the threshold for ion detection is the same as Fig. 5. At the highest energies we have considered, as many as 20 alkali-metal sites had to be included to get convergence in the P_{N}. The net results are shown in Fig. 6. For F/LiF(100), the results appear reasonable however P_{N} is decreasing much too rapidly at high energy. Partly this is due to the use of an H atom mass rather than an F atom mass. This is entirely consistent with RN being a Demkov process. We can write the diabatic transfer probability as

$$P = \tfrac{1}{2}\mathrm{sech}^2\left(\frac{\pi\Delta E}{2\gamma v}\right), \tag{36}$$

where v is the velocity of the projectile. Increasing the mass simply decreases v, which in turn leads to smaller probabilities for curve-hopping. This mass dependence is not enough to correct the P_{N} completely. We can see that for F/KI(100), the discrepancy is very large and occurs at much lower energies, because the PESs are much closer in energy.

What is clear from this example of a possible RN path is that we must consider more than three PESs to describe the net effect of the atom–surface reaction. Especially for the F/KI system, with its lower workfunction and band-gap, we can expect the ion to be formed and re-neutralized many times over at higher energies. Each time this occurs, there will be some energy cost to be paid from

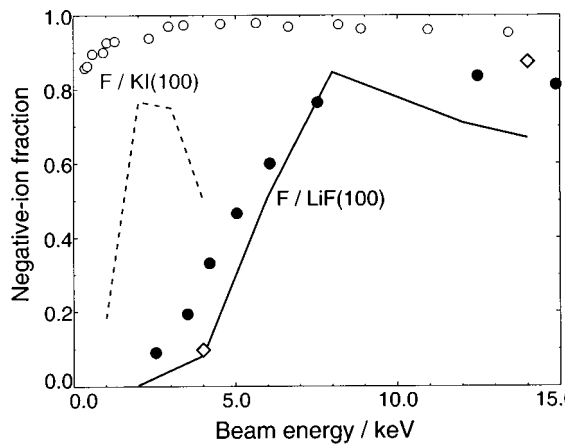

Fig. 6 Net negative-ion fraction *vs.* incident beam energy when re-neutralization by charge transfer into the conduction band is included. The lines represent theoretical results using a mass of 1 u, filled (open) circles represent experimental results for LiF(100) (KI(100)) and the open diamonds represent theoretical results for a projectile mass of 4 u.

the translational motion. At the very highest energies, it is impossible to say whether the atom will end-up as a negative or a neutral. Most likely then the decline of P_N observed in experimental results between $\sim$20 and 100 keV is due to a decrease in probability of the initial ion formation stage. This remains to be tested by further calculation.

V. Conclusions

We have presented a diabatic description of the charge exchange reaction occuring between atoms and alkali-metal surfaces, deriving PESs with a flexible and consistent semi-empirical scheme and solving the atom motion with exact wavepacket dynamics. For the F/LiF(100) system, we find a curve-crossing between the PESs for (neutral atom, neutral surface) and (negative ion, positive surface) configurations. There is efficient charge transfer, in fact the initial ion-formation probability is unity. At lowest energies, these ions fail to escape from the surface promptly. If we count only the fraction which do escape on the first bounce, we obtain an ion detection probability behaving very similarly to that of experiment. Increasing the angle of incidence moves the threshold to lower energy, and the threshold energy is lower for a surface with a lower workfunction, as we have demonstrated for the F/KI(100) system, in agreement with experiment. In future work, we shall examine the importance of the curve-crossing to the dynamics, and try to establish the fate of the trapped negative ions.

Acknowledgements

This work was supported in part by a British Council—Israel Ministry of Science Fellowship for GRD.

References

1 R. Brako and D. M. Newns, *Rep. Prog. Phys.*, 1989, **52**, 655.
2 J. Los and J. J. C. Geerlings, *Phys. Rep.*, 1990, **190**, 133.
3 C. Auth, A. G. Borisov and H. Winter, *Phys. Rev. Lett.*, 1995, **75**, 2292.
4 H. Winter, A. Mertens, C. Auth and A. G. Borisov, *Phys. Rev. A*, 1996, **54**, 2486.
5 H. Winter, C. Auth and A. G. Borisov, *Nucl. Instrum. Methods Phys. Res. B*, 1996, **115**, 133.
6 C. Auth, A. Mertens, H. Winter, A. G. Borisov and V. Sidis, *Phys. Rev. A*, 1998, **57**, 351.
7 S. Ustaze, R. Verucchi, S. Lacombe, L. Guillemot and V. A. Esaulov, *Phys. Rev. Lett.*, 1997, **79**, 3526.
8 S. Ustaze, L. Guillemot, R. Verucchi, S. Lacombe and V. A. Esaulov, *Nucl. Instrum. Methods. Phys. Res. B*, 1998, **135**, 319.
9 A. Mertens, C. Auth, H. Winter and A. G. Borisov, *Phys. Rev. A*, 1997, **55**, R846.
10 A. G. Borisov, V. Sidis and H. Winter, *Phys. Rev. Lett.*, 1996, **77**, 1893.
11 A. G. Borisov and V. Sidis, *Phys. Rev. B*, 1997, **56**, 10628.
12 V. Sidis, *Adv. Chem. Phys.*, 1992, **82**, 135.
13 J. M. Adams, S. Evans and J. M. Thomas, *J. Phys. C*, 1973, **6**, L382.
14 A. B. Kunz, *Phys. Rev. B*, 1982, **26**, 2056.
15 G. K. Wertheim, J. E. Rowe, D. N. E. Buchanan and P. H. Citrin, *Phys. Rev. B*, 1995, **51**, 13675.
16 Y. Zeiri and M. Shapiro, *Chem. Phys.*, 1978, **31**, 217.
17 Y. Zeiri, M. Shapiro and R. Tenne, *Chem. Phys. Lett.*, 1983, **99**, 11.
18 M. Shapiro and Y. Zeiri, *J. Chem. Phys.*, 1986, **85**, 6449.
19 Y. Zeiri, R. Tenne and M. Shapiro, *J. Chem. Phys.*, 1984, **80**, 5283.
20 F. O. Ellison, *J. Am. Chem. Soc.*, 1963, **85**, 3540.
21 H. A. Pohl, R. Rein and K. Appel, *J. Chem. Phys.*, 1964, **41**, 3385.
22 G. R. Darling, R. Kosloff and Y. Zeiri, in preparation.
23 R. Pariser, *J. Chem. Phys.*, 1953, **21**, 568.
24 R. S. Mulliken, C. A. Rieke, D. Orloff and H. Orloff, *J. Chem. Phys.*, 1949, **17**, 1248.
25 W. A. Steele, *The Interaction of Gases with Solid Surfaces*, Pergamon, New York, 1974, ch. 2.
26 R. Heather and H. Metiu, *J. Chem. Phys.*, 1994, **86**, 5009.
27 G. J. Kroes and R. C. Mowrey, *J. Chem. Phys.*, 1994, **101**, 805.
28 H. Tal-Ezer and R. Kosloff, *J. Chem. Phys.*, 1984, **81**, 3967.
29 R. Kosloff, in *Numerical Grid Methods and Their Application to the Schrödinger Equation*, ed. C. Cerjan, Kluwer, Amsterdam, 1997, p. 175.
30 J.-P. Gauyacq, personal communication.
31 Yu. N. Demkov, *Sov. Phys. JETP*, 1964, **18**, 138.